Multi-disciplinary and multi-objective optimization problem applied to a morphing blade cascade study

Giada AbateⒾ **and Johannes Riemenschneider**

Abstract
Multi-disciplinary design optimization (MDO) problems incorporate a number of coupled disciplines that need to be simultaneously solved to achieve a complete solution. Such problems are common in turbomachinery blade design, where MDO usually integrates constraints coming from aerodynamics and structural mechanics. In the present work, a multi-disciplinary and multi-objective optimization problem is formulated and applied to a morphing blade cascade study. An aero-structure coupling strategy is also integrated in the framework to take into account the interactions between aerodynamics and structural mechanics. The morphed blade geometry is obtained by means of a shape memory alloy (SMA) actuator that morphs and adapts the blade leading-edge shape to the inflow conditions in order to improve the aerodynamic flow characteristics, and therefore the overall cascade performance. A surrogate-based optimization strategy is applied to find the Pareto points representing the optimal blade configurations in terms of total pressure loss coefficient at design and off-design conditions. Results show a decrease up to 55% in the total pressure loss coefficient at the off-design condition with a Young's modulus of about 100 GPa and an actuator length between 30 and 45 mm.

1 Introduction

A multi-disciplinary problem involves several disciplines that are usually coupled and must be solved together in order to achieve a complete solution. In the past, multi-disciplinary design optimization (MDO) has been successfully applied to turbomachinery design (Panchenko et al., 2003; Idahosa et al., 2008; Ampellio et al., 2016; Jha, 1999) to integrate in the problem definition not only aero- and thermodynamic performance of turbines and compressors, but also geometrical requirements, mechanical integrity, and manufacturing costs Dornberger et al., 2020. Of particular interest are the turbomachinery applications involving constraints coming from critical disciplines like aerodynamics and structural mechanics into the design process. Even though there is a strong interaction between aero-structural effects, several studies consider these two disciplines independent to avoid the burden of coupling the respective numerical solvers. For instance, Talya et al. (2000) integrated aerodynamic and heat transfer design objectives along with blade geometry constraints, and developed a multi-disciplinary optimization procedure for gas turbine blade design. Talya et al. evaluated the aerodynamic loads by a Navier-Stokes solver, and calculated the interior temperature with a finite element analysis (FEA). Those aerodynamic and structural results were finally combined into a single MDO framework. Another example is available in Dornberger et al. (2020) where the authors developed an automated multi-disciplinary optimization environment that provides a generic interface to external software (i.e. computational fluid-dynamic (CFD) and FEA). Kosuke et al. (2004) used an inverse design method combined with CFD and FEA to optimize the performance of a centrifugal compressor and a radial turbine stage of a microturbine system. Leonid et al. (2004) conceived an optimization approach based on reduced order models to optimize the design of axial turbine blades with the final goal of achieving stage maximal efficiency meeting both stress-strain and

German Aerospace Center (DLR), Braunschweig, Germany

Data Availability Statement included at the end of the article

Corresponding author:
Giada Abate, German Aerospace Center (DLR), Lilienthalpl. 7, Braunschweig, 38108, Germany.
Email: giada.abate@dlr.de

vibration reliability requirements. Pierret et al. (2006) combined the use of a genetic algorithm (GA) with an approximate model to accelerate the optimization process of the NASA Rotor 67 at three different operative conditions. Verstraete et al. (2007) coupled a GA with an artificial neural network approach to optimize a radial compressor for micro gas turbine application using a 3D Navier-Stokes solver and FEA. All the works mentioned above describe multi-disciplinary optimization problems without a coupling strategy between the disciplines involved; indeed, results coming from different solvers are analyzed separately neglecting the interactions between them.

However, in the turbomachinery blade design, aerodynamics and structural mechanics are highly coupled disciplines: aerodynamic loads generate stresses and strains in the blade structure resulting in deformations that in turn affect the aerodynamics itself. Moreover, it is generally not recommended to use low-fidelity flow solvers in such problems because they are not accurate in the prediction of flow separation. Therefore, it is necessary to use high-fidelity flow solvers which however, are computationally expensive. Luo et al. (2009) studied transonic compressor blades, and developed an automatic multi-objective optimization approach using parallel multi-objective differential evolution (MDE) algorithms combined with a non-uniform B-Spline method to couple Reynolds-Averaged Navier-Stokes (RANS) solutions with FEA. The B-Spline method is a load surface technique able to transfer the aerodynamic loads from the RANS solver to the finite element analysis Lizhou Li (2006). In particular, this coupling approach transfers the loads by a Bi-cubic B-Spline surface fitted from the CFD results in a parametric space where both CFD and FEA nodes are mapped Lizhou Li (2006). When considering morphing aeronautical elements, the coupling between aerodynamics and structural mechanics becomes even more important since these two disciplines impose contrasting requirements to the design process. On one hand, the structure has to be stiff enough to withstand the aerodynamic loads while maintaining the prescribed aerodynamic properties; on the other hand, it has to be compliant enough to allow shape changes. The result is a compromise between the two requirements. For this purpose, several fluid-structure interaction (FSI) methods have been developed to achieve a more complete and reliable design process of morphing devices Ricci and Terraneo (2006); Potsdam et al. (2006); Heinrich R. (2008); Gamboa et al. (2009); Molinari et al. (2011, 2014), but all of these techniques are conceived to be used with purely three-dimensional or two-dimensional solvers, that is, CFD and FEA are both either 3D or 2D. However in a blade cascade application, the 3D CFD analysis can be simplified by considering its equivalent 2D problem in order to reduce the computational costs. At this point, the aero-structure coupling has to link

the 2D CFD analysis with the three-dimensional structural model resulting in a 2D-3D coupling, where the 2D CFD computational grid is matched with the 3D FEA mesh in order to transfer the aerodynamic loads from the CFD analysis to the structural model. Such a strategy has been presented and successfully tested in Abate et al. (2021).

As mentioned before, high-fidelity flow solvers are necessary to well predict flow separation but they negatively affect the computational time. In the field of design optimization with computationally expensive function evaluation, surrogate-based optimizers are some of the most suitable algorithms in order to reduce the number of required function evaluations to identify the possible global optimum. While the previous publication (Abate et al. (2021)) only describes the multi-disciplinary coupling, in the present work, the 2D-3D fluid-structure interaction framework is integrated in a multi-objective optimization problem where a surrogate-based approach is implemented to minimize the total pressure loss coefficient of a morphing blade cascade. The blade leading-edge geometry is morphed by means of a shape memory alloy (SMA) actuator placed on the pressure side of the blade, whose actuation adapts the nose shape to the inflow conditions Abate et al. (2021). The resulting design variables are the blade Young's modulus, and the dimensions and location of the morphing device. More information about blade geometry, SMA modeling, and CFD and FEA settings are provided in Abate et al. (2021). In the following sections, a detailed description of the optimization problem will be presented. In particular, Section 2 provides a description of the blade geometry and the morphing device; in Section 4, there is an overview of the optimization framework, and a detailed presentation of the optimization problem and the algorithm implemented. Section 5 shows the final results; and finally, the conclusion (Section 6) summarizes the described work and the relevant results achieved.

2. Geometry and flow conditions

As detailed described in Abate et al. (2021), the baseline cascade blade geometry is generated from the DLR SC14-067 Reutter et al. (2014, 2017) airfoil coordinates provided by the Institute of Propulsion Technology - Department of Fan and Compressor of the German Aerospace Center (DLR). The cascade has an airfoil chord length of 70 mm and span of 120 mm (Figure 1).

A shape memory alloy actuator is integrated in the blade pressure side surface (Figure 1) in order to deform and adapt the blade leading-edge accordingly to the inflow conditions. In particular, the actuator is activated by heating the SMA up leading to a contraction of the material fibers – according to the material properties – and therefore, to a bending of the blade
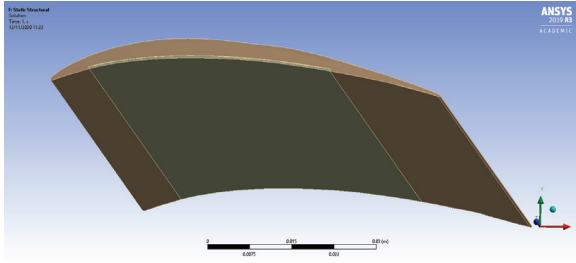
Figure 1. Baseline blade geometry with the actuator on the pressure side.

Figure 2. Airfoil cascade Abate et al. (2021).

leading-edge. More details about the SMA model implemented in this work are presented in Abate et al. (2021).

Other flow properties to consider are the inlet Mach number of 0.65, and the inflow angle β_1 (Figure 2) of 134 deg at the design condition where the flow over the blade is mostly attached to the body surface (Figure 3(a)). On the other hand at off-design conditions ($\beta_1 = 138$ deg), the inflow angle increases, and a flow separation may appear on the blade suction side (Figure 3(b)) leading to a degradation in the cascade performance. In order to reduce these negative effects, the SMA actuator is activated to move downwards the blade leading-edge (Figure 4), thereby obtaining a reduction of the inlet metal angle with a consequent improvement of the aerodynamic flow characteristics.

The SMA actuator has a thickness of 0.4 mm, and the starting and ending x-coordinates of the actuator (Figure 5) along the blade are the design variables of the optimizer, as detailed described in the next section.

3. FEA and CFD overview

A quick overview of the FEA and CFD analysis is given in this section. A detailed presentation of the simulation settings is available in Abate et al. (2021).

3.1 FEA

The finite element analysis is conducted in Ansys Workbench®. Aluminum alloy material is assigned to the blade, and shape memory alloy to the actuator. A simplified approach has been used to model the SMA considering the complexity of the aero-structural coupling. Therefore, the SMA has been modeled as an isotropic material with linear material behavior. Moreover, martensite and austenite stiffness as well as the hysteresis have not been taken into account., and the actuation of the SMA has been considered only in one direction. The actuation of the SMA has been considered only in one direction (chordwise direction) such that when a temperature is assigned to the material, the actuator contracts in that direction leading to
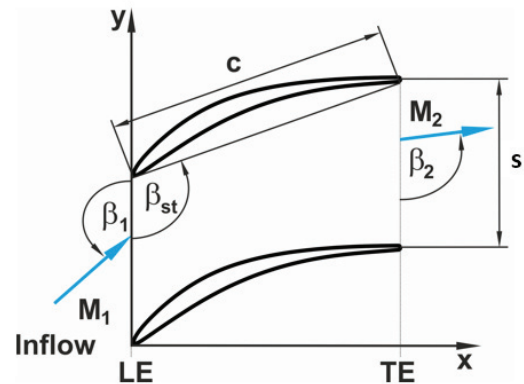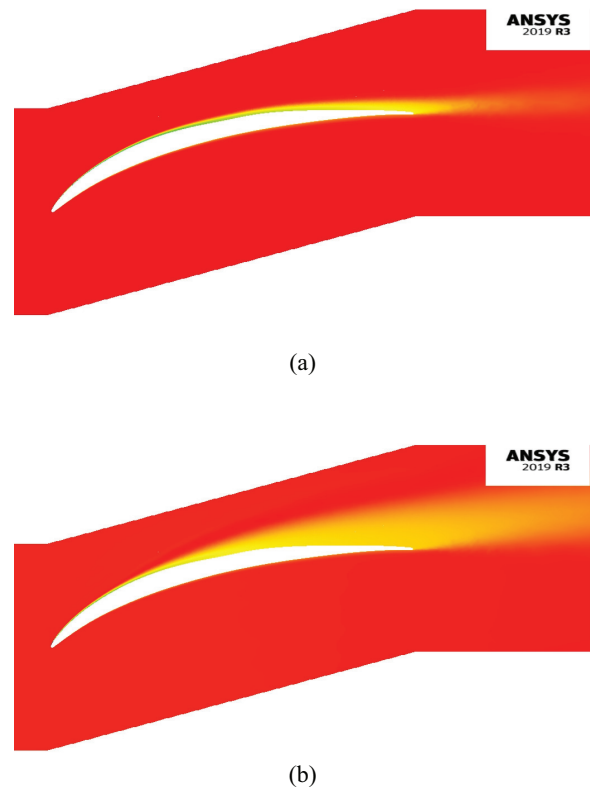

Figure 3. Total pressure at design and off-design conditions for the baseline blade Abate et al. (2021): (a) Design condition and (b) Off-design condition.

a downward bending of the blade leading-edge. As just mentioned, the SMA needs a thermal condition to be activated. This is modeled by using a thermal analogy that simulates the voltage on the actuator leading to its activation. In particular, a temperature of 100°C is considered for the active actuator, while 0°C corresponds to zero strain.
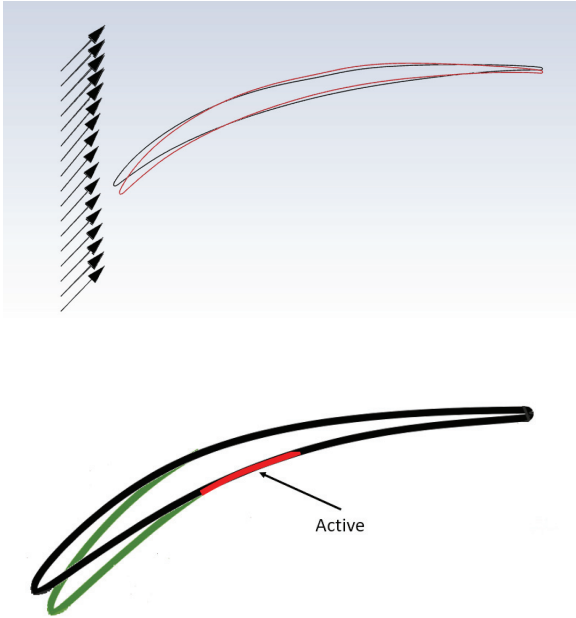
Figure 4. Downwards displacement of the blade leading-edge due to the SMA actuator Abate et al. (2021).
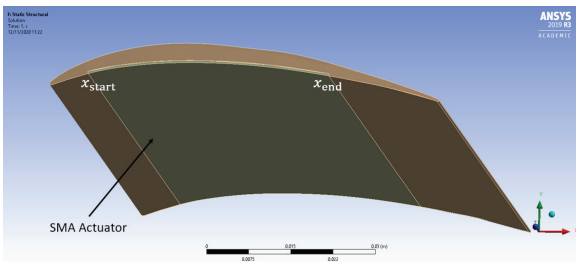
Figure 5. x-coordinates of the SMA actuator.

3.2 CFD

The computational fluid-dynamic analysis has been carried out in Ansys Fluent®. It has been decided to consider a simple two-dimensional problem to reduce the computational cost. The flow conditions have been already described in the previous section and more details can be found in Abate et al. (2021). The mesh is quadrilateral with 30 prism layers close to the airfoil surface in order to have a wall $y+ < 1$. After a grid independence study, the final mesh results to have about 150,000 elements. The flow is steady, compressible, and fully turbulent; the $k - \omega$ shear stress transport (SST) turbulence model has been selected and coupled with a $y+ < 1$ in order to solve the entire boundary layer. Two outputs of the CFD analysis are saved and used for the fluid-structural coupling: 2D mesh and pressure distribution over the airfoil.

3.3 Fluid-structure interaction framework

The fluid-structure interaction (FSI) framework integrated into the optimization process couples the 2D structural analysis with the 3D aerodynamic problem. A schematic representation of the FSI method is shown in Figure 6. The process starts with the geometry generation of the 3D baseline blade with the SMA actuator on the pressure side. This 3D geometry and the original 2D airfoil shape are used in the FEA and CFD analysis, respectively. The challenging point in the FSI framework lies on the "mesh matching" phase where the 3D structural mesh coming from the FEA is matched with the 2D CFD one such that the aerodynamic loads associated with the CFD mesh nodes can be transferred to the structural ones. The resulting "matched" FEA nodes with the associated aero-loads are transferred to the structural analysis which returns both the deformed blade geometry and the new mesh as output. The steps presented above are then repeated again in an iterative process that stops when the difference in the leading-edge displacement along the y-axis between to consecutive iterations is less than $2 \ 10^{-5}$ [m].

A detailed description of all the FSI phases is presented in Abate et al. (2021).

4. Multi-objective optimization problem

4.1 Problem formulation

The goal of this work is to maximize the performance of a morphing blade cascade by changing the leading-edge shape in order to adapt the blade geometry to the inflow conditions. In particular, the optimization problem searches for the morphed blade configurations that minimize the total pressure loss coefficient ω both at design and off-design conditions by changing the Young's modulus of the blade material (E_{blade}), x_{start}, and x_{end} of the SMA actuator. The total pressure loss coefficient ω is defined as:

$$\omega = \frac{p_{01} - \bar{p}_{02}}{q_1} \quad (1)$$

where p_{01} is the total pressure at the cascade inlet, $\bar{p}_{02}$ is the area-weighted average total pressure at outlet, and q_1 is the dynamic pressure at inlet. A reduction of ω means a reduction in the pressure losses, and therefore, an enhancement in the cascade aerodynamic performance. As introduced before, both design and off-design conditions are considered in this study, and for this reason, the objective function ω must be minimized at both design (ω_{des}) and off-design (ω_{off}) conditions. Therefore, the resulting optimization problem is a multi-objective problem where ω_{des} and ω_{off} are the two objective functions. Even though no morphing occurs at the design condition, it is important to evaluate the
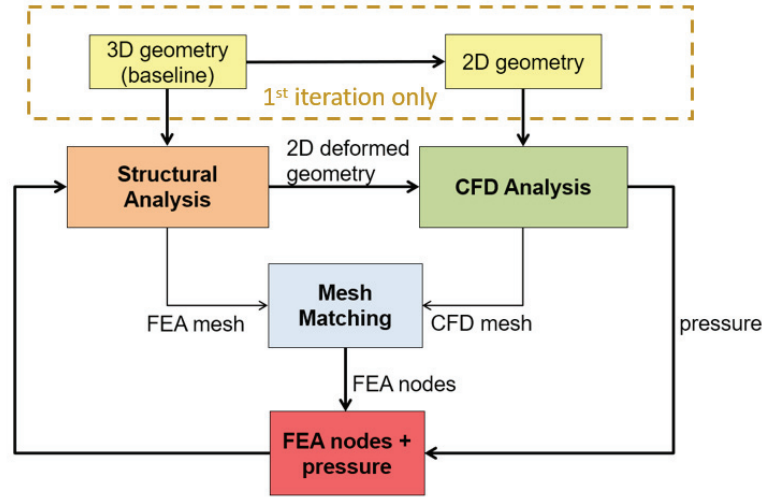
Figure 6. Schematic representation of the FSI method. Abate et al. (2021).

value of ω even at this operative point because the presence of the SMA actuator changes the structural property of the blade, therefore affecting the geometry and the aerodynamic performance of the loaded blade. It is well known that the result of a multi-objective optimization problem is given by a set of non-dominated solutions that define the so-called Pareto front; for the specific problem presented in this paper, the Pareto points represent the morphed blade configurations with optimized performance in terms of total pressure loss coefficient at design and off-design conditions. The formulation of the multi-objective problem solved in this paper can be stated as follow:

$$\text{minimize:} \quad f_1(\text{x}) = \omega_{\text{des}}(\text{x}) \quad (2)$$

$$f_2(\text{x}) = \omega_{\text{off}}(\text{x}) \quad (3)$$

$$\text{by changing:} \quad \text{x} = [x_{\text{start}}, x_{\text{end}}, E_{\text{blade}}] \quad (4)$$

$$\text{subject to:} \quad 0.1c \leq x_{\text{start}} \leq 0.5c \quad (5)$$

$$0.6c \leq x_{\text{end}} \leq 0.9c \quad (6)$$

$$70 \cdot 10^9 [Pa] \leq E_{\text{blade}} \leq 300 \cdot 10^9 [Pa] \quad (7)$$

where c is the chord length, x_{start} and x_{end} are the starting and ending actuator coordinates (Figure 5), and E_{blade} is the blade Young's modulus measured in Pa. Geometric constraints are applied to the actuator x-coordinates (equations (5,6)) in order to keep feasible the resulting blade configurations, and an additional constraint is also considered for the Young's modulus of the blade material (equation 7).

Such a problem can be solved with a genetic algorithm or with a surrogate-based approach. Because of the high computational costs of the analysis tools (CFD and FEA) involved in the process, it has been decided to implement a surrogate-based optimization,

in particular the MATLAB®surrogate-based algorithm together with the ϵ-constraint technique in order to tackle the multi-objective formulation of the problem. The ϵ-constraint approach is known to be well suited for multi-objective problems with two objectives like the one presented in this article. Therefore, the number of resulting single objective problems to solve exponentially increases with the number of objective functions, thereby making problems with more than two objectives intractable with such a technique.

4.2 ϵ-constraint method

The ϵ-constraint approach finds an accurate discrete representation of the Pareto front of the multi-objective optimization solution by minimizing a primary objective ($f_1(x)$), and bounding the other objectives ($f_2(x)$) in the form of inequality constraints with decreasing limits. Therefore considering f_1 and f_2 equal to ω_{des} and ω_{off}, respectively, the previous optimization problem can now be formulated as follow:

$$\text{minimize:} \quad f_1(x) = \omega_{\text{des}}(x)$$

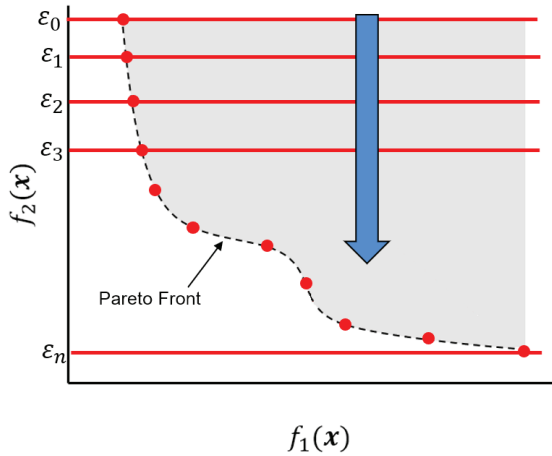$$\text{subject to:} \quad \omega_{\text{off}}(x) \leq \epsilon$$

$$0.1c \leq x_{\text{start}} \leq 0.5c$$

$$0.6c \leq x_{\text{end}} \leq 0.9c$$

$$70 \cdot 10^9 \leq E_{\text{blade}} \leq 300 \cdot 10^9$$

where an additional constraint on ω_{off} is added in order to exclude from the solution all the points in the design space that do not satisfy that specific constraint. Figure 7 shows an example of the ϵ-constraint method: starting from a given value of ϵ (i.e. ϵ_0), the first run of the ϵ-constraint method excludes from the solution all the points in the design space that do not satisfy the
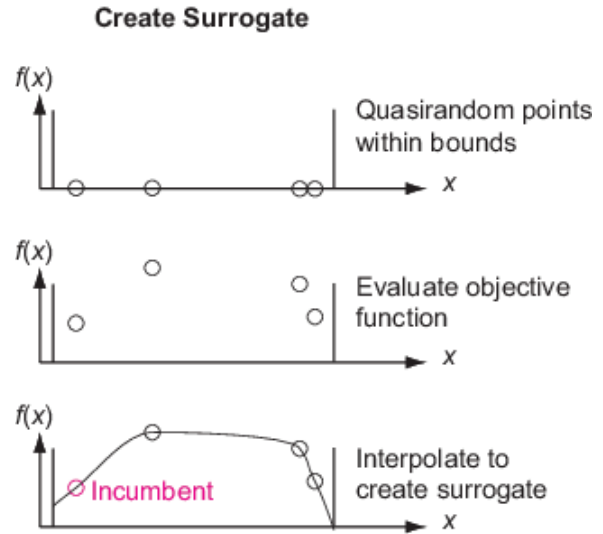
Figure 7. Example of the ϵ-constraint approach.

(a)

(b)

Figure 8. The two phases of the MATLAB®surrogateopt function MATLAB (2018): (a) Phase 1 and (b) Phase 2.

condition $f_2(x) \leqslant \epsilon_0$, in other words all the points above the red line. Therefore, by running a single-objective optimization for $f_1(x)$, it is possible to find the first Pareto point on the red line passing through ϵ_0. The second step consists in changing the value of ϵ (for example ϵ_1 in the figure) in order to move downwards the search for all the Pareto points. The process is repeated for all the selected ϵ values. The number and the value of ϵ constraints should be defined by the user with the goal of obtaining a uniform discrete representation of the Pareto front. In particular, the extreme values ϵ_0 and ϵ_n correspond to f_2 evaluated at the optimal designs resulting from the single objective optimization of f_1 and f_2, respectively.
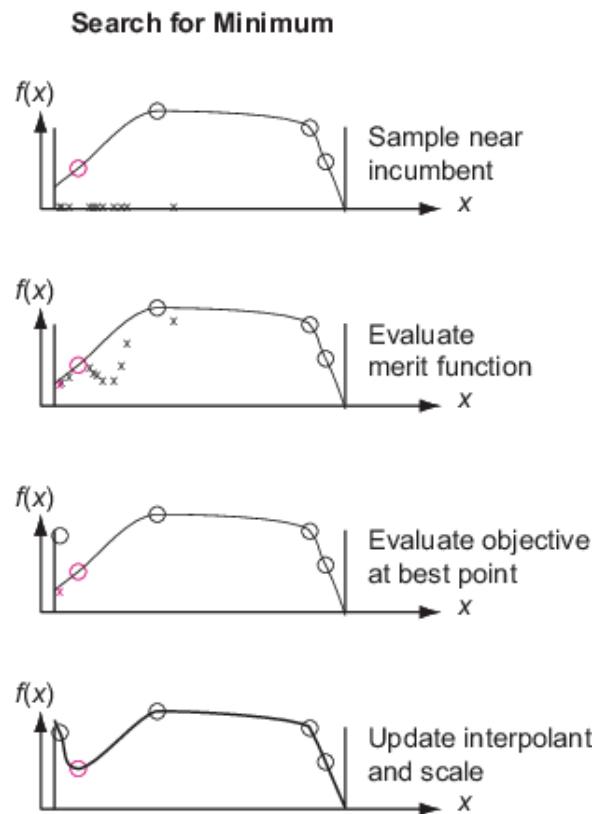
4.3 Surrogate-based optimization

The single-objective problem resulting from the ϵ-constraint method is solved by the surrogate-based optimizer *surrogateopt* available in MATLAB®. In the first phase, the algorithm takes random points within the bounds and evaluates the objective function $f(x)$ at these points. Then, it constructs the initial surrogate of $f(x)$ by interpolating a radial basis function through these points (Figure 8(a)). In the second phase (Figure 8(b)), a merit function – which is based on the surrogate model MATLAB (2018)– is evaluated at several thousand locations that are randomly sampled in a trust region around the incumbent best point. The random sample returning the lower merit function is chosen as a candidate for the evaluation of $f(x)$ in order to update the surrogate and search again. The trust region boundaries are updated and the process is repeated until convergence is reached. More details about the MATLAB® *surrogateopt* algorithm can be found in MATLAB (2018).

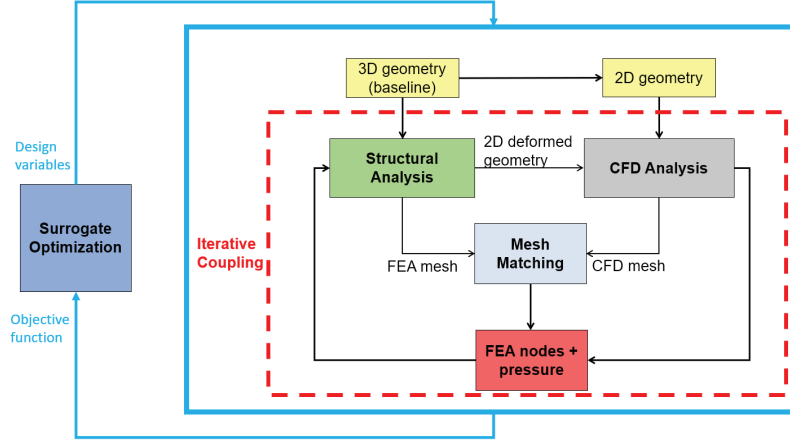The non-linear constraint given by the ϵ-constraint method is included in the optimization algorithm via an external penalty function assigned to the objective function f_1. In particular, recalling that f_1 is the total pressure loss coefficient evaluated at the design condition (ω_{des}), and f_2 is ω_{off} which is the objective function

Figure 9. Schematic representation of the optimization process with the integrated FSI framework.

ω evaluated at the off-design condition, the optimization problem is reformulated in the following way:

$$
\begin{aligned}
\text{minimize:} \quad & \tilde{\omega}_{\text{des}} \\
\text{subject to:} \quad & 0.1c \leqslant x_{\text{start}} \leqslant 0.5c \\
& 0.6c \leqslant x_{\text{end}} \leqslant 0.9c \\
& 70 \cdot 10^9 \leqslant E_{\text{blade}} \leqslant 300 \cdot 10^9
\end{aligned}
$$

where $\tilde{\omega}_{\text{des}}$ is the penalized objective function defined as:

$$
\tilde{\omega}_{\text{des}} = \omega_{\text{des}} + \psi(\omega_{\text{des}}, \epsilon) \tag{8}
$$

$$
= \omega_{\text{des}} + \left(\left(0, \frac{k(\omega_{\text{off}} - \epsilon)}{\epsilon} \right) \right)^2 \tag{9}
$$

with $k = 100$, and the second addend representing the penalty function. When the constraint for ω_{off} is satisfied, the penalty function is 0, and therefore, $\tilde{\omega}_{\text{des}}$ is simply equal to the original ω_{des}; whereas when $\omega_{\text{off}} > \epsilon$, $\tilde{\omega}_{\text{des}}$ is the new penalized objective function in order to exclude from the solution all the points that do not satisfy the constraint.

4.4 Multi-disciplinary problem

As mentioned before, the performance analysis of a morphing blade cascade involves two highly coupled disciplines: aerodynamics for the load evaluation, and structural mechanics to calculate stresses and deformations due to both aero-loads and actuator. Therefore, it is highly important to create a connection between CFD and FEA solvers such that they can exchange information and results to achieve a complete solution of the overall performance analysis. An aero-structure coupling method has been developed in Abate et al. (2021) where a 2D CFD analysis is linked to a 3D

structural solver by matching the 2D CFD mesh nodes with the 3D structural grid in order to transfer the aerodynamic loads and find the corresponding deformed blade shape. This 2D-3D aero-structure coupling tool is now integrated in the multi-objective optimization framework presented in the previous sections. In Figure 9, a schematic representation of the optimization loop with the iterative aero-structural coupling is shown. The optimizer gives the design variables as input to the fluid-structure interaction (FSI) framework; those define the characteristics of each blade configuration in terms of Young's modulus of the blade material, and dimensions and location of the SMA actuator. The resulting blade is then simulated in both CFD and FEA solvers inside the FSI process where the aerodynamic analysis gives the aero-loads to the structural model and the structural analysis returns the deformed blade geometry due to both aero-loads and actuator effect. This deformed shape goes back to the CFD solver, and the iterative loop between aerodynamic and structural analyses is repeated until convergence. More details about the FSI framework are given in Abate et al. (2021). The iterative loop between CFD and FEA returns the values of the two objective functions (ω_{des}, ω_{off}) needed by the optimizer for the function evaluation.

5. Results

The Pareto front resulting from the multi-objective problem is plotted in Figure 10 that reports the variation of the total pressure loss coefficient in percentage evaluated at design and off-design conditions. In particular, the performance variation of the i-th geometry is calculated as the difference between ω of the simulated morphed blades and ω of the baseline blade (original undeformed blade without actuators):
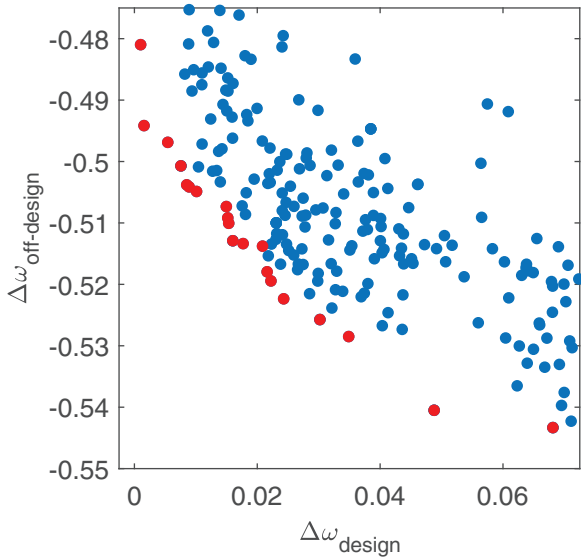
Figure 10. Pareto front and total pressure loss variation plot.
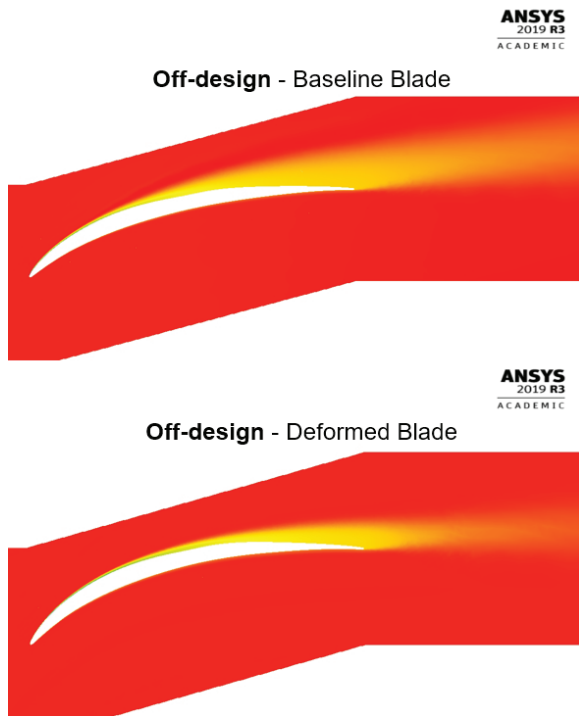
Figure 11. Total pressure on baseline and morphed blades at the off-design condition Abate et al. (2021).

$$\Delta\omega_i = \frac{\omega_i - \omega_{\text{base}}}{\omega_{\text{base}}} 100 \qquad (10)$$

where ω_i is the ω of the optimization case i, and ω_{base} is the baseline ω value. As mentioned, the $\Delta\omega$ is calculated at both design and off-design conditions, and plotted on the x and y axes in Figure 10. In this figure, each dot represents a case generated by the optimizer and simulated in the aero-structural coupling loop; the red

points are the solution of the multi-objective optimization problem namely the Pareto points. As it is possible to see, all the blade configurations in the Pareto front show an expected but negligible increase in the total pressure loss coefficient at the design condition; on the other side, a relevant performance improvement is noticeable at the off-design condition where the total pressure loss coefficient decreases up to 55%. This is due to the improved aerodynamic characteristics of the flow showing a delayed separation on the suction surface of the morphed blade compared to the original one. Indeed, the morphing leading-edge makes it possible to adapt the blade shape to the inflow conditions in order to modify the inlet metal angle of the blade and to decrease the flow separation originally due to a high incidence angle. An example of the morphing effects on the flow characteristics at off-design conditions is given in Figure 11 where the total pressure is plotted for both baseline (undeformed) and a morphed blade with a decrease in the loss coefficient of about 50%.

The solution of the multi-objective optimization problem gives also important insights into actuator length and Young's modulus of the blade material. In particular, Figure 12 shows that an actuator length between 30 and 45 mm is the best choice to get a reduction of the total pressure loss coefficient especially at off-design conditions; moreover, the most promising length to achieve a good compromise between design and off-design results seems to be of about 30 mm. About the value of the Young's modulus, Figure 13 shows that most of the blades on the Pareto front are characterized by a value of about 100 GPa which is a common value for the Titanium alloys.

6. Conclusion

In the present work, a multi-disciplinary and multi-objective optimization problem has been applied to a morphing blade cascade study. In particular, an aero-structural coupling strategy previously developed Abate et al. (2021) has been integrated in the optimization framework in order to consider the interactions between aerodynamics and structural mechanics in the cascade performance analysis. An SMA actuator on the pressure side of the blade has been used as morphing device to bend the blade leading-edge downwards in order to adapt the shape to the inflow conditions leading to an improvement in the aerodynamic characteristics of the flow, and therefore, in the overall cascade performance. In this study, it has been decided to work only with one morphing device at the bottom blade surface since it has been noticed a positive aerodynamic effects when the blade is bent downwards; however in some circumstances, aerodynamic improvements can be achieved also by bending the blade upwards, and therefore, by activating an SMA actuator
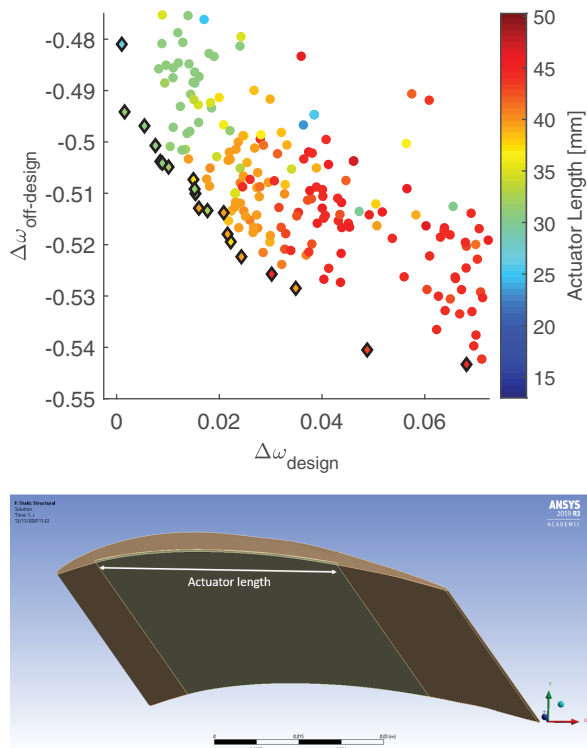
Figure 12. Actuator length results.
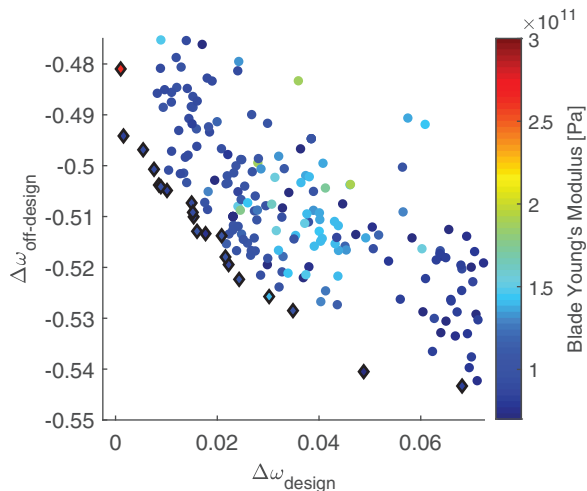
Figure 13. Blade Young's modulus results.

on the suction side of the blade. This is part of planned future works. The optimization problem has been set to minimize the total pressure loss coefficient at both design and off-design conditions, and considering the Young's modulus of the blade material, and the dimensions and location of the actuator as design variables. Because of the high computational costs of the analysis tools (CFD and FEA) involved in the process, the multi-objective problem has been successfully solved by means of a surrogate-based optimization (MATLAB®

surrogateopt) with the ϵ-constraint method and penalty function. The solution shows a relevant decrease up to 55% in the total pressure loss coefficient at off-design conditions when the blades are characterized by a Young's modulus of about 100 GPa, and an actuator length between 30 and 45 mm.

Declaration of conflicting interests

The authors declared no potential conflicts of interest with respect to the research, authorship, and/or publication of this article.

Funding

ORCID iD

Giada Abate https://orcid.org/0000-0002-4320-4447

Data availability statement

Data sharing not applicable to this article as no datasets were generated or analyzed during the current study.

References

Abate G, Riemenschneider J and Hergt A (2021) Aero-structural coupling strategy for a morphing blade cascade study. *ASME Journal of Turbomachinery* 144: 061002. DOI:10.1115/1.4053174.

Ampellio E, Bertini F, Ferrero A, et al. (2016) Turbomachinery design by a swarm-based optimization method coupled with a cfd solver. *Advances in Aircraft and Spacecraft Science* 3(2): 149.

Luo C, Liming S, Jun L, et al. (2009) Multiobjective optimization approach to multidisciplinary design of a three-dimensional transonic compressor blade. *ASME Turbo Expo 2009: Power for Land, Sea and Air*.

Dornberger R, Stoll P and Büche D. (2020). *Multidisciplinary turbomachinery blade design optimization*. American Institute of Aeronautics and Astronautics .

Gamboa P, Vale J, Lau FJP, et al. (2009) Optimization of a morphing wing based on coupled aerodynamic and structural constraints. *AIAA Journal* 47(9): 2087–2104. DOI: 10.2514/1.39016.

Heinrich RNJ and Kroll N (2008) *Fluid-structure coupling for aerodynamic analysis and design: A dlr perspective*. AIAA Aerospace Sciences Meeting and Exhibit .

Idahosa U, Golubev VV and Balabanov VO (2008) An automated optimal design of a fan blade using an integrated cfd/mdo computer environment. *Engineering Applications of Computational Fluid Mechanics* 2(2): 141–154.

Jha R (1999) *Development of multidisciplinary design optimization procedures for smart composite wings and turbomachinery blades*. Arizona State University.

Watanabe H, Okamoto H, Guo S, et al. (2004) *Optimization of microturbine aerodynamics using cfd, inverse design and fem structural analysis: 1st report—compressor design*. ASME Turbo Expo 2004: Power for Land, Sea and Air.

Moroz L, Govoruschenko Y, Romanenko L, et al. (2004) *Methods and tools for multidisciplinary optimization of axial turbine stages with relatively long blades.* ASME Turbo Expo 2004: Power for Land, Sea, and Air.

Li L (2006) *Turbine blade temperature transfer using the load surface method.* Elsevier.

MATLAB (2018) https://de.mathworks.com/help/gads/surrogate-optimization-algorithm.html

Molinari G, Arrieta AF and Ermanni P (2014) Aerostructural optimization of three-dimensional adaptive wings with embedded smart actuators. *AIAA Journal* 52(9): 1940–1951. DOI:10.2514/1.J052715.

Molinari G, Quack M, Dmitriev V, et al. (2011) Aero-structural optimization of morphing airfoils for adaptive wings. *Journal of Intelligent Material Systems and Structures* 22(10): 1075–1089. DOI:10.1177/1045389X11414089.

Panchenko V, Moustapha H, Mah S, et al. (2003) *Preliminary multi-disciplinary optimization in turbomachinery design.* Technical report, PRATT AND WHITNEY CANADA CORP LONGUEUIL (QUEBEC).

Pierret S, Filomeno Coelho R and Kato H (2006) Multidisciplinary and multiple operating points shape optimization of three-dimensional compressor blades. *Structural and Multidisciplinary Optimization* 33(1): 61–70. DOI: 10.1007/s00158-006-0033-y.

Potsdam M, Yeo H and Johnson W (2006) Rotor airloads prediction using loose aerodynamic/structural coupling. *Journal of Aircraft* 43(3): 732–742. DOI:10.2514/1.14006.

Reutter O, Hemmert-Pottmann S, Hergt A, et al. (2014) Endwall contouring and fillet design for reducing losses and homogenizing the outflow of a compressor cascade. In: *Turbo Expo: Power for Land, Sea, and Air*, volume 45608. American Society of Mechanical Engineers, p. V02AT37A007.

Reutter O, Rozanski M, Hergt A, et al. (2017) Advanced endwall contouring for loss reduction and outflow homogenization for an optimized compressor cascade. *International journal of turbomachinery, Propulsion and Power* 2(1): 1.

Ricci S and Terraneo M (2006) Application of mdo techniques to the preliminary design of morphed aircraft. *AIAA/ISSMO Multidisciplinary Analysis and Optimization Conference* DOI:10.2514/6.2006-7018.

Verstraete T, Alsalihi Z and Van den Braembussche R (2007) *Multidisciplinary optimization of a radial compressor for micro gas turbine applications.* ASME Turbo Expo 2007: Power for Land, Sea and Air.

Talya S, Chattopadhyay A and Rajadas J (2000) *An integrated multidisciplinary design optimization procedure for cooled gas turbine blades.* American Institute of Aeronautics and Astronautics DOI:10.2514/6.2000-1664.